Newsletters on Stratigraphy, Vol. 57/2 (2024), 153–170
Published online January 31, 2024; published in print April 2024

Improved chronostratigraphy for the Messel Formation (Hesse, Germany) provides insight into early to middle Eocene climate variability

Stefanie Kaboth-Bahr[1,2]*, Clemens Schmitt[3,4], Thorsten Bauersachs[2], Christian Zeeden[5], Thomas Wonik[5], Jonas Schandl[2], Olaf Lenz[6,7], Sonja Wedmann[8], Iuliana Vasiliev[3], Andreas Mulch[3,4], Lucas Lourens[9], Jörg Pross[2] and André Bahr[2]

With 6 figures and 3 tables

Abstract. Besides providing unique information on early mammal evolution, the UNESCO World Heritage Site "Messel Fossil Pit" (Hesse, Germany) yields detailed insight into short-term climate variability during the early to middle Eocene due to its annually laminated oil-shale sequence. Here, we constrain the chronostratigraphy of the sediments from the Messel paleolake to allow precise correlation with other marine and terrestrial archives from that time period. This study utilizes a suite of geochemical proxy data (gamma ray, total organic carbon and carbon isotopes of organic matter) obtained from a scientific drillcore (FB2001) from the depocenter of the Messel paleolake. The drillcore comprises the full succession of the lacustrine sediments of the Lower (LMF) and ~60 % of the Middle Messel (MMF) Formations, including all marker beds that are used to stratigraphically correlate excavated fossil remains across the lake basin. Based on the proposed astronomical tuning, we infer that the LMF and MMF obtained in core FB2001 cover in total c. 840 kyr and were deposited between 48.06 Ma and 47.22 Ma. More specifically, our tuning yields a duration of c. 130 kyr and c. 430 kyr for the annually laminated oil shale of the LMF and MMF, respectively. Our results imply a slightly longer deposition of the LMF than previously proposed based on the same core. By contrast, the deposition of the MMF occurred over a slightly shorter time interval. As a result of our tuning approach, and considering the revision of a previously published $^{40}Ar/^{39}Ar$ age for the base of the LMF, the top of the MMF in core FB2001 has an age of 47.22 ± 0.21 Ma and is thus ~200 kyr younger than suggested previously. We also find that the average sedimentation rate (~20 cm/kyr) for the oil-shale intervals is slightly higher than previously estimated. In line with previously published palynological records our geochemical data point to a strongly variable climate during deposition of the LMF and MMF, with humidity changes being paced by orbital precession and eccentricity. The synchronicity of negative excursions in the organic matter-derived carbon-isotope signals for the LMF and MMF as presented in our study to those registered in quasi-global

Authors' addresses:
[1] Institute of Geological Sciences, Freie Universität Berlin, Malteserstrasse 74-100, 12249 Berlin, Germany
[2] Institute of Earth Sciences, Heidelberg University, Im Neuenheimer Feld 234-236, 69120 Heidelberg, Germany
[3] Senckenberg Biodiversity and Climate Research Centre, Senckenberganlage 25, 60325 Frankfurt, Germany
[4] Institute of Geosciences, Goethe University Frankfurt, Altenhöferallee 1, 60438 Frankfurt, Germany
[5] LIAG – Leibniz Institute for Applied Geophysics, Stilleweg 2, 30655 Hannover, Germany
[6] Senckenberg Research Institute and Natural History Museum Frankfurt, Senckenberganlage 25, 60325 Frankfurt, Germany
[7] Institute of Applied Geosciences, Technical University Darmstadt, Schnittspahnstraße 9, 64287 Darmstadt, Germany
[8] Senckenberg Research Station Grube Messel, Senckenberg Research Institute and Natural History Museum Frankfurt, Markstraße 35, 64409 Messel, Germany
[9] Department of Earth Sciences, Utrecht University, Princetonlaan 8a, 3584 CB Utrecht, The Netherlands
* Corresponding author: stefanie.kaboth-bahr@fu-berlin.de

DOI: 10.1127/nos/2024/0799
Borntraeger Science Publishers, Stuttgart, www.borntraeger-cramer.com

carbon-isotope compilations further corroborates the robustness of our age model. As these quasi-global carbon-isotope anomalies represent disturbances of the global carbon cycle and are often associated with abrupt warming events ("hyperthermals"), the organic-rich sediments recovered at Messel provide the opportunity to study the response of aquatic and terrestrial ecosystems to climate disturbances in unprecedented temporal resolution.

Key words. Messel Pit Fossil Site, Middle Eocene, astrochronology, hyperthermals

1. Introduction

Due to rising greenhouse-gas concentrations the Earth system currently moves toward climate states without historic precedent, challenging societal adaptation (IPCC 2021). However, Earth's geological history offers possible analogues that cover individual aspects of the warming world of the coming decades. Thus, studying such past climates can be instrumental for fine-tuning model predictions and ultimately support our abilities for adaption to future climate change. Past analogues of future climate conditions include the climatic state of the early Eocene (c. 56–47.8 Ma; Bijl et al. 2013), which based on current greenhouse-gas emission trajectories will likely be reached in ~2150 (Burke et al. 2018). During the early Eocene, global mean annual surface temperatures were 13.0 ± 2.6 °C higher than those of the late 20th century (Caballero and Huber 2013), high latitudes were characterized by near-tropical warmth and lacked ice shields (Sluijs et al. 2009, Pross et al. 2012), and the atmospheric carbon dioxide (pCO_2) level was at approximately 1,400 parts per million volume, i. e., more than three times higher than today (Anagnostou et al. 2016, Rae et al. 2021).

The maar-lake sediments of the Messel Pit Fossil Site, an UNESCO world heritage site in the State of Hesse, Germany, provide an exceptional sedimentary archive to study early to middle Eocene climate variability (Fig. 1). Deposited c. 48 Ma ago, the Messel oil shale is famous for its exceptionally well-preserved vertebrate, insect, and plant fossils that provide a spectacular glimpse into terrestrial ecosystems of the Paleogene (e. g., Schweizer et al. 2007, Smith et al. 2018, Wedmann et al. 2007, Wedmann et al. 2021). Its sediments also represent a unique archive for investigating short-term climate dynamics operating in the mid-latitudes (assuming a middle Eocene paleolatitude of ~46° N for Messel; Smith et al. 2018) during the geologically most recent greenhouse period of the Earth. While the early and middle Eocene has formerly been viewed as climatically relatively stable (Pearson et al. 2007, Kozdon et al. 2011), high-resolution benthic oxygen and carbon-isotope data reveal that it has been punctuated by a number of hyperthermals characterized by pronounced, negative carbon-isotope excursions that point at recurring large-scale disturbances of the global carbon cycle (Zachos et al. 2010, Westerhold et al. 2020).

This study revisits and improves the currently available astronomical tuning of the research drillcore FB2001 retrieved from the depocenter of the former Messel maar lake. For this purpose, we utilized downhole gamma-ray data together with results from a suite of time-series analyses. The improved age model allows for a better temporal placement of the LMF and MMF within the early to middle Eocene time scale, thus providing the basis to link regional climate variability as documented at Messel to global climate dynamics. While there is now a robust understanding of Eocene climate variability and carbon-cycle dynamics from marine records (Westerhold et al. 2020), regional-scale time-equivalent continental climate archives as provided by Messel are yet scarce. Hence, the revised record will be instrumental for improving our understanding of continental climate variability as well as providing a basis to ground-truth numerical models that simulate Eocene climate (e. g., Zhu et al. 2019).

2. Study area and the FB2001 drillcore

The Messel pit is located close to the city of Darmstadt near the Upper Rhine Graben (Fig. 1), a prominent central segment of the Cenozoic Central European Rift System (e. g., Illies 1972, Hinsken et al. 2007). Like Messel, there are about half a dozen isolated outcrops of Paleogene sediments on the structural high formed by the Sprendlinger Horst, which is the northern extension of the Variscan Odenwald basement (Fig. 1). As most of the other Paleogene occurrences on the Sprendlinger Horst, the succession at Messel represents the remnant of a maar crater filled by basal volcaniclastics that are overlain by lacustrine strata

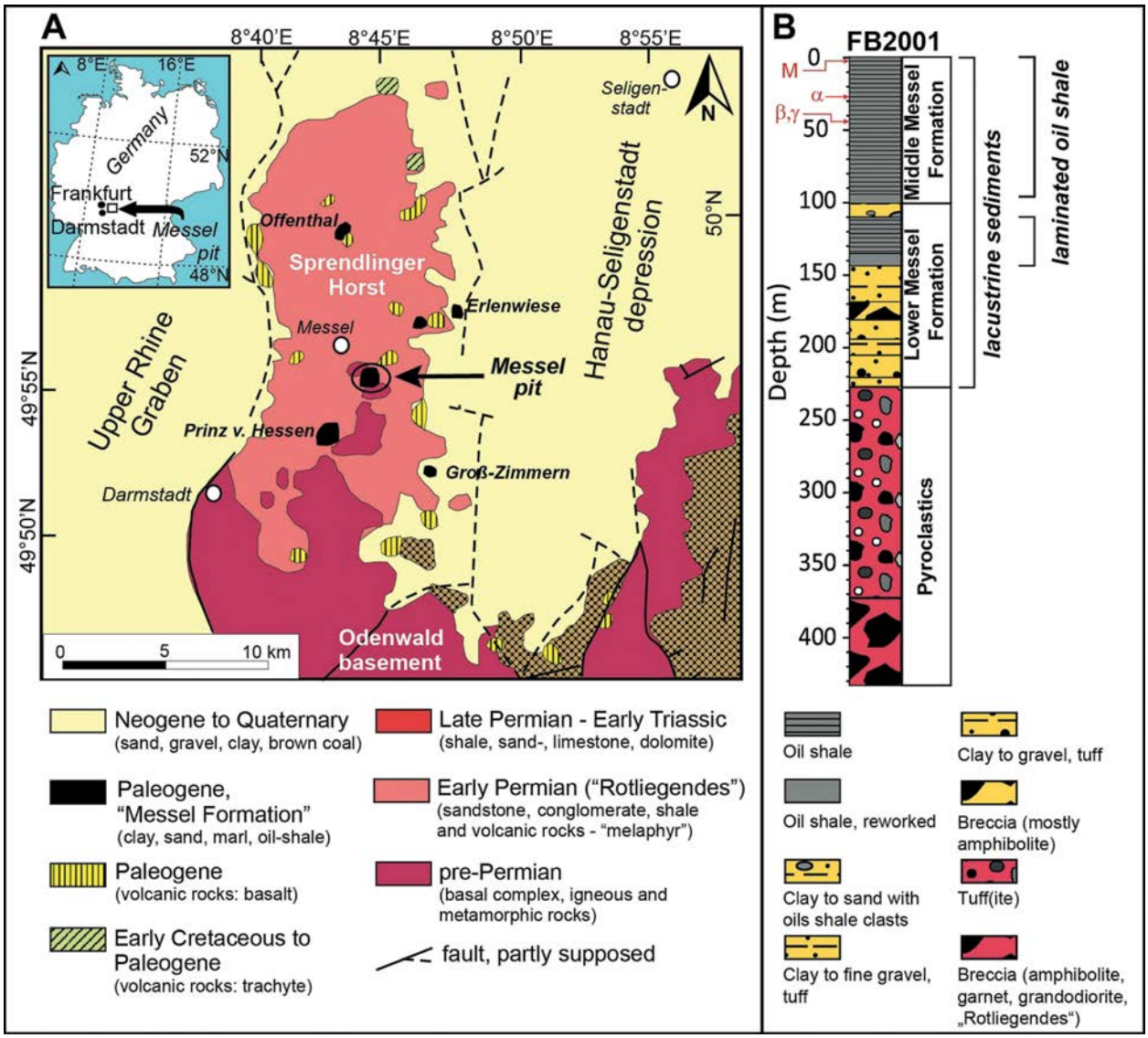

Fig. 1. **(A)** Geological map showing the location of the Messel Pit in relation to other Paleogene sites in the area (modified after Harms et al. 1999); (**B**) generalized lithostratigraphy of the Messel FB2001 drillcore (modified after Felder and Harms 2004) with the position of the marker beds indicated (orange; cf. Section 2 for more details).

(Schulz et al. 2002). In order to obtain a continuous succession of the Eocene strata at Messel, the research core FB2001 was drilled in 2001 in the depocenter of the former Messel maar lake (Schulz et al. 2002; Fig. 1). The drillcore penetrated the lacustrine succession and reached the underlying volcaniclastic rocks and vent breccia. As such, it provided evidence that the maar lake was formed by phreatomagmatic eruptions (Schulz et al. 2002, Lorenz 2003, Felder and Harms 2004). A basaltic clast from the volcanoclastic material immediately underlying the oil-shale deposit at 267.8 m depth (Mertz and Renne 2005) has been dated to 48.27 ± 0.22 Ma and 48.11 ± 0.22 Ma by $^{40}Ar/^{39}Ar$ (Lenz et al. 2015), respectively, depending on the presumed age of the reference material. This date has previously been used as a chronostratigraphic anchor for the overlying lacustrine strata (Lenz et al. 2015).

The initial lacustrine phase of the Messel maar lake in the FB2001 drillcore consists of the LMF (228–111 m core depth; Fig. 1), which comprises abundant mass-movement deposits that formed due to oversteepened crater walls (Schulz et al. 2002, Felder and Harms 2004). While the lake in its early stages was holomictic, increasing stability of the crater walls and successive deepening of the lake led to the intermittent

establishment of meromictic conditions reflected by the deposition of finely laminated bituminous shale ("oil shale") in the upper part of the LMF (143-111 m core depth; Fig. 1, Felder and Harms 2004). Separated from this lower oil-shale interval by a horizon of reworked sediments (111–94 m core depth), the classic "Messel oil shale" of the MMF commences at 94 m core depth (Fig. 1). It consists of finely laminated bituminous claystones that provide evidence for stable meromictic conditions in the lake (Felder and Harms 2004; Fig. 1). The sub-mm-scale alternation of light and dark laminae of the oil shale reflects a quasi-annual varve-like stratification (Goth 1990, Goth et al. 1988, Irion 1977, Lenz et al. 2011). It is estimated that the total thickness of the MMF at the FB2001 drillsite amounted to ~155 m before economic excavation of the oil shale started (Felder & Harms 2004); hence, the drillcore comprises ~60 % of the originally deposited MMF.

Within the MMF, four marker horizons (from stratigraphically oldest to youngest: γ, β, α, and M; Fig. 1) are commonly used for inter-basinal correlation and serve as reference horizons to determine the relative stratigraphic position of fossil remains. Marker horizons α, β, and γ were first defined by Franzen et al. (1982). Marker horizon M (named after the mineral montgomeryite; Schaal et al. 1987) is situated at 3.91 m core depth and consists of up to 0.3 cm thick tripartite layers of phosphate minerals, with bands of messelite ($Ca_2Fe^{2+}(PO_4)_2 \cdot 2H_2O$) crystals enclosing a montgomeryite-rich band (e. g., Schaal et al. 1987, Felder and Harms 2004, Liesegang and Wuttke 2022). Marker horizon α ('gray layer'), located at 27.36 m core depth, is a fine sand with a quarzitic matrix and a thickness between 0.1 and 1.0 cm. Marker horizon β ('double mica horizon'), found at 42.4 m core depth, consists of highly decomposed feldspar and mica and has a thickness of ca. 2 cm. Marker horizon γ ('white layer'), located at 44.4 m core depth, is a clay layer with a characteristic bright weathering color and a thickness of ~0.2 cm. Marker beds β, α and M have been tentatively interpreted as diagenetically altered tephra layers (Weber 1988, Liesegang and Wuttke 2022). The FB2001 core has recovered all of these marker horions, thus enabling the chronostratigraphic placement of fossils found at Messel. This is also important in a wider regional context as the recovered mammal remains are used to stratigraphically constrain other terrestrial Eocene strata in Central Europe (Ring et al. 2020). The overlying Upper Messel Formation is not contained in the FB2001 core because it had already been removed due to previous mining activity and is today only preserved as remnants along the former margins of the Messel maar lake (Felder and Harms 2004).

Paleontological and palynological evidence suggests that the surroundings of the Messel maar lake during the deposition of the LMF and MMF were covered by paratropical vegetation (Lenz et al. 2011). A long-term trend towards drier conditions was overprinted by repeated changes in floral composition that have been argued to be driven by orbital forcing (Lenz et al. 2010, Lenz et al. 2011, Lenz et al. 2015). Based on the assignment of precession, obliquity, and eccentricity to the dominant periods in the power spectrum of the palynological data, an astronomical age model was developed by Lenz et al. (2015), which indicated that the deposition of the entire 94 m of the MMF in the FB2001 core occurred over ~640 kyr (corresponding to a mean sedimentation rate of ~14 cm/kyr). Such a sedimentation rate would support the hypothesis that the lamination of the oil-shale indeed represents annual lamination (Irion 1977, Goth et al. 1988, Goth 1990, Lenz et al. 2010, Lenz et al. 2015). Based on the absolute ages of the underlying volcanoclastic rocks (48.27 ± 0.22 Ma and 48.11 ± 0.22 Ma; see above) combined with orbital tuning, Lenz et al. (2015) proposed that the MMF as preserved in the FB2001 drillcore was deposited between approx. 48.3 Ma and 47.6 Ma.

The palynological data of Lenz et al. (2015) have a temporal resolution of ~1.4 kyr, which allows identifying potential orbital cyclicities. However, their dependence on multiple environmental variables (e. g., temperature, precipitation, and seasonality), each responding differently to an external forcing such as insolation, complicates tuning to an appropriate astronomical solution and thus hampers the development of a more robust, astronomically anchored stratigraphy (Lenz et al. 2015). A recent re-calibration of the $^{40}Ar/^{39}Ar$ reference standard (Phillips et al. 2022) furthermore necessitates revisiting the chronostratigraphic anchoring of the sedimentary succession found at Messel.

3. Material and methods

3.1. Gamma-ray data

Gamma-ray logging is used to predict the varying lithology in borehole by measuring the spontaneous emission of gamma radiation from rocks (Nazeer et al.

2016). We here use the regular spaced downhole gamma-ray log data (vertical sample rate = 0.1 m) from drillhole FB2001 for the depth interval between 190 m and 1 m as previously published by Felder and Harms (2004) and Wonik (2005). We linearly detrended and step-wise (window size = 30 m) z-score normalized the gamma-ray data using the functions znorm and rollapplyas implemented in the *dprep* (Acuna et al. 2009) and *zoo* R package (Zeileis and Grothendieck 2005). The "normalized" gamma-ray data, hereafter simply referred to as gamma-ray data, were then used for the subsequent time-series analysis (cf. Section 3.3 for more details). The original gamma-ray log data are shown in Supplementary Figure 1.

3.2. Total Organic Carbon (TOC) content

To assess the relationship between gamma-ray log variability and changes in organic-matter content, we analyzed ten samples from the FB2001 depth interval 10–9 m for their TOC content. This new dataset (Fig. 2, Table 1, Table 2) is supplementary to the TOC record of Bauersachs et al. (2014) for the depth interval 145–1 m of the same core. The new samples were measured due to low spatial resolution of the existing TOC data set (~two samples per meter; Bauersachs et al. 2014) relative to the gamma-ray data (~10 data points per meter), and thus allow for a same-resolution assessment of the gamma-ray/TOC relationship based on an exemplary selected 1 m core section of FB2001. For the TOC measurements, we followed the protocol of Bauersachs et al. (2014). In short, the dried and powdered sediment samples (ca. 30 mg) were pretreated with excess 2M hydrochloric acid (HCl) to remove carbonates, neutralized with distilled water, and again dried at 50 °C for 24 h. Subsequently, samples were measured in duplicates using a CS-Analyser 144DR (Leco Corporation) at the Institute of Earth Sciences at Heidelberg University with an analytical precision of repeated measurements better than 0.5 %.

3.3. Time-series analysis

Due to the presumed debris-flow deposition concurrent with the clastic layers at 228–143 m and 111–94 m core depth (Felder and Harms 2004; cf. Fig. 1 and Section 2 for more details), we excluded these depth intervals from the subsequent time-series analysis of the gamma-ray data.

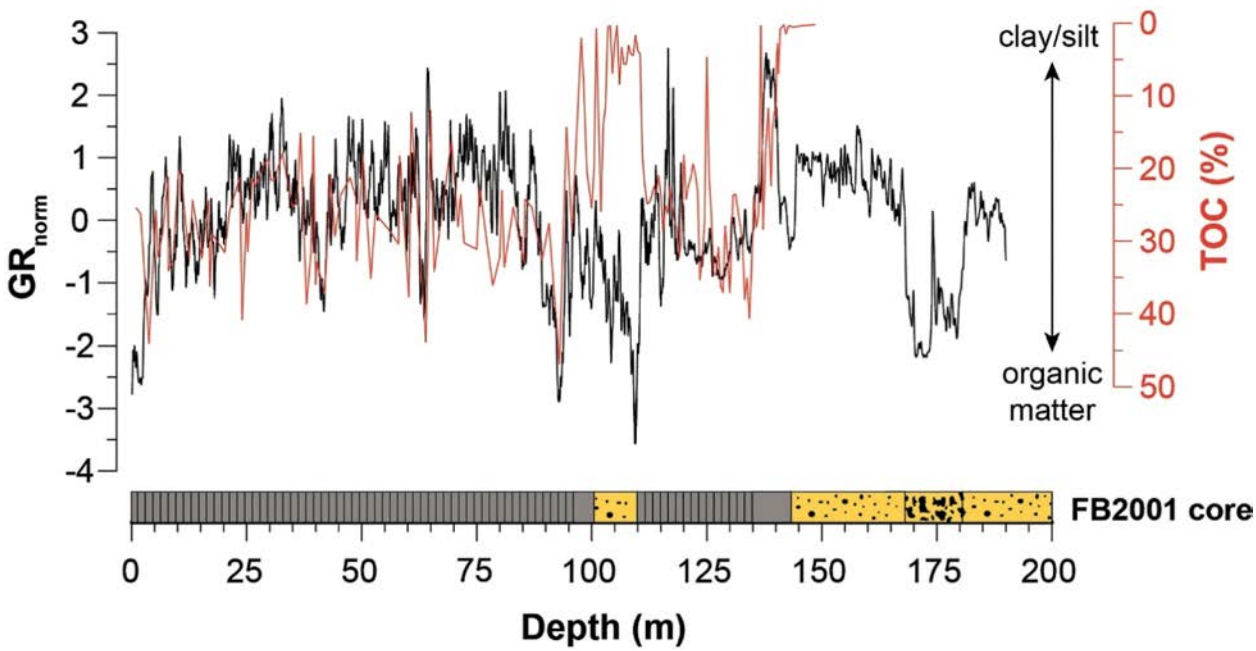

Fig. 2. Comparison of the "normalized" gamma-ray downhole log data (GR) from the FB2001 drillcore (black line; Felder and Harms 2004; cf. Section 3 for more details) at Messel with the total organic carbon (TOC) data (red line) from the FB2001 sediment core (Bauersachs et al. 2014, and this study; cf. Section 3 for more details). The generalized lithostratigraphy of the Messel FB2001 drillcore (after Felder and Harms 2004) is also shown horizontally (see Fig. 1 for more information).

Table 1. Age-depth tie points of the applied astronomical tuning of the Lower and Middle Messel Formation recovered from the FB2001 drillcore to the La2010d astronomical target (Laskar et al. 2011).

Drillcore Depth (m)	Age (Ma) La2010d
1.00	47.22
7.40	47.25
16.80	47.31
24.90	47.35
44.00	47.44
52.00	47.48
62.00	47.53
89.10	47.63
94.00	47.65
111.00	47.70
144.00	47.86
228.00	48.06

Table 2. Total organic carbon (TOC) content of selected samples from the FB2001 drillcore (cf. Fig. 2 and Section 3.2 for more details).

Drillcore Depth (m)	TOC (%)
9.08	35.08
9.17	37.06
9.24	41.96
9.38	39.42
9.40	37.18
9.52	36.38
9.58	31.45
9.75	32.13
9.80	33.01
9.87	26.28

To investigate the potential imprint of orbital cyclicities (e. g., precession, obliquity and eccentricity) of the gamma-ray data of the oil-shale intervals from drillhole FB2001, we utilized the REDFIT algorithm (Schulz and Mudelsee 2002) implemented in PAST 4.10 (Hammer et al. 2001) and evolutive harmonic spectrum analysis (EHA) implemented in the *astrochron* package in R (Meyers 2014, R Core Team 2014). In particular, EHA is an extremely powerful spectral analysis approach as it aids the identification of potential sedimentation-rate changes.

To test the robustness of the identified orbital cyclicities an Average Spectral Misfit (ASM) analysis was carried out to assign dominant spectral peaks derived from the gamma-ray data to the orbital frequency bandwidths utilizing the *astrochron* R software package (Meyers 2014). The applied taner filter as implemented in the *astrochron* R software package (Meyers 2014) and herein utilized for the astronomical tuning of the LMF and MMF was centered at 1/3.65 and had a roll-off rate of 10^5.

3.4. Bulk organic carbon isotope analysis

To increase the spatial resolution of the $\delta^{13}C_{TOC}$ record of Bauersachs et al. (2014), which encompasses the 145–1 m depth interval of the FB2001 drillcore, additional 25 samples from the depth interval between 146 and 1 m (Tab. 3) were analyzed for their $\delta^{13}C_{TOC}$ values following the protocol of Bauersachs et al. (2014). In short, portions of the powered, decalcified sediment samples (1–2 mg) were analyzed for $\delta^{13}C_{TOC}$ using a Flash Elemental Analyzer 1112 (Thermo Scientific), connected to the continuous flow inlet system of a MAT 253 gas-source mass spectrometer (Thermo Scientific) at the Joint Goethe University-Senckenberg BiK-F Stable-Isotope Facility, Goethe

Table 3. Bulk organic carbon ($\delta^{13}C_{TOC}$) isotope values of selected samples from the FB2001 drillcore (cf. Fig. 6 and Section 3.4 for more details).

Drillcore Depth (m)	$\delta^{13}C_{TOC}$ (‰ VPDB)
1.48	–30.7
2.28	–30.5
4.88	–29.6
11.49	–29.3
21.48	–29.4
27.28	–29.4
27.38	–29.3
31.48	–28.4
36.88	–28.7
42.28	–26.5
42.38	–27.5
42.47	–26.7
48.78	–29.2
48.88	–29.2
49.08	–28.7
55.08	–27.3
61.48	–26.8
81.48	–25.7
91.79	–28.9
92.59	–26.8
117.50	–26.9
125.50	–26.5
131.25	–25.8
140.00	–31.2
146.00	–26.1

University Frankfurt. Carbon isotopes in graphite standard USGS24 were analyzed alongside the samples in order to monitor accuracy and precision. The isotope ratio is expressed in conventional delta notation: δ_{sample} (‰) = [($R_{sample} - R_{standard}$)/$R_{standard} - 1$] × 1000, where R is the ratio of $^{13}C/^{12}C$ of the sample and the standard Vienna Pee Dee Belemnite (VPDB). Accuracy and precision of all isotopic analyses were determined by replicate sample analysis, which yielded pooled standard errors better than 0.2 ‰ for $\delta^{13}C_{TOC}$.

4. Results and discussion

4.1. Gamma-ray and TOC data

The gamma-ray signal of the FB2001 sediments shows a distinct cyclical pattern (cf. Section 4.2 for more details) in the oil-shale sections of the LMF and MMF. Notably, the variability of the gamma-ray signal is inversely correlated to the TOC signal for the oil-shale intervals (Fig. 2). The anticorrelation between the TOC and gamma-ray signals indicates a dilution effect: this scenario, K- and Th-rich clays in the oil shale contribute to a high gamma-ray signal (Díaz-Curiel et al. 2021, Poupon and Gaymard 1970), while high TOC contents lead to its dilution. This implies that organic substances, which due to their high U content usually yield high gamma-ray signals (Fertl and Chilingar 1988, Raddadi et al. 2005), are a less important gamma-ray source than clay minerals in the Messel oil shale. Interestingly, gamma-ray and TOC signals correlate positively for the interval dominated by coarse clastics between 111 and 94 m (Fig. 2). In this case, it appears that the more quartz-rich coarse clastics dominating this interval (Felder and Harms 2004) are a low gamma-ray source relative to TOC, leading to a higher gamma-ray signal when TOC is high.

The variations of the downhole gamma-ray signal of the oil shale can be either interpreted as fluctuation in TOC production and preservation or as changes in the detrital, clay-rich input into the Messel paleolake. Both scenarios would result in varying amounts of clay vs. TOC content as manifested in the gamma-ray signal. As detailed in Section 4.2, we argue that the fluctuations in the gamma-ray signal reflect orbitally driven changes in precipitation that led to varying detrital input into the lake. This interpretation is supported by the lack of evidence for cyclical changes in TOC production by algal blooms in the lake (Lenz et al. 2011). We further have no indication that the meromicitic state of the lake, and hence oxygenation state of the lake bottom affecting organic matter preservation, underwent distinct changes throughout the deposition of the oil-shale intervals of the LMF and MMF (Bauersachs et al. 2014, Schulz et al. 2002). It thus appears that the gamma-ray signal is foremost a reflection of detrital material influx to the Messel paleolake, driven by changes in precipitation (Lenz et al. 2015, Lenz and Wilde 2018). The dominance of one environmental factor (i. e., precipitation) in shaping the proxy signal makes the gamma-ray record of the FB2001 sediment core an ideal target of astronomical tuning.

4.2. Astronomical tuning KBSB 2022 of the FB2001 sequence for the early to middle Eocene

The assessment of the gamma-ray data for both oil-shale intervals from drillcore FB2001 shows significant cycles in the Redfit-spectrum (Fig. 3) at ~6.7 m, ~4.2 m, ~2.3 m, and ~1.8 m band-widths for the LMF (143–111 m drillcore depth), and at ~5.6 m, ~4.6 m, ~3.6 m, ~3.0 m, and ~2.4 m band-widths for the MMF (94–0 m drillcore depth), respectively. Comparable cycles for the oil-shale interval of the MMF have also been noted in the FB2001 pollen data (Lenz et al. 2015). Assuming sedimentation rates between 10 and 50 cm/kyr, which is in accordance with previous estimates based on pollen data and laminae counting (Goth 1990, Lenz et al. 2010, Lenz et al. 2015), we assessed the potential relationship of these significant cycles from the depth domain to orbital frequencies of the half-precession (1/11), precession (1/19 and 1/21), obliquity (1/41), and short and long eccentricity (1/100, 1/400) frequency range given their presence in the initial astronomical tuning of Lenz et al. (2015). Based on the applied ASM analysis (Fig. 3; cf. Section 3.3 for more details), we find that the significant ~2.3 m and ~1.8 m depth cycles of the LMF presumably relate to half-precession, while the ~4.2 m cycle seems to be a reflection of orbital precession. Additionally, the documented ~6.7 m cycle, which based on the calculated average sedimentation rate of ~21 cm/kyr for the oil shale of the LMF (Fig. 3) translates into a ~32 kyr cycle, could potentially reflect a weak obliquity signal or a non-linear component (Lourens et al. 2010, Hodell et al. 2023). Based on the ASM analysis and the calculated average sedimentation rate of

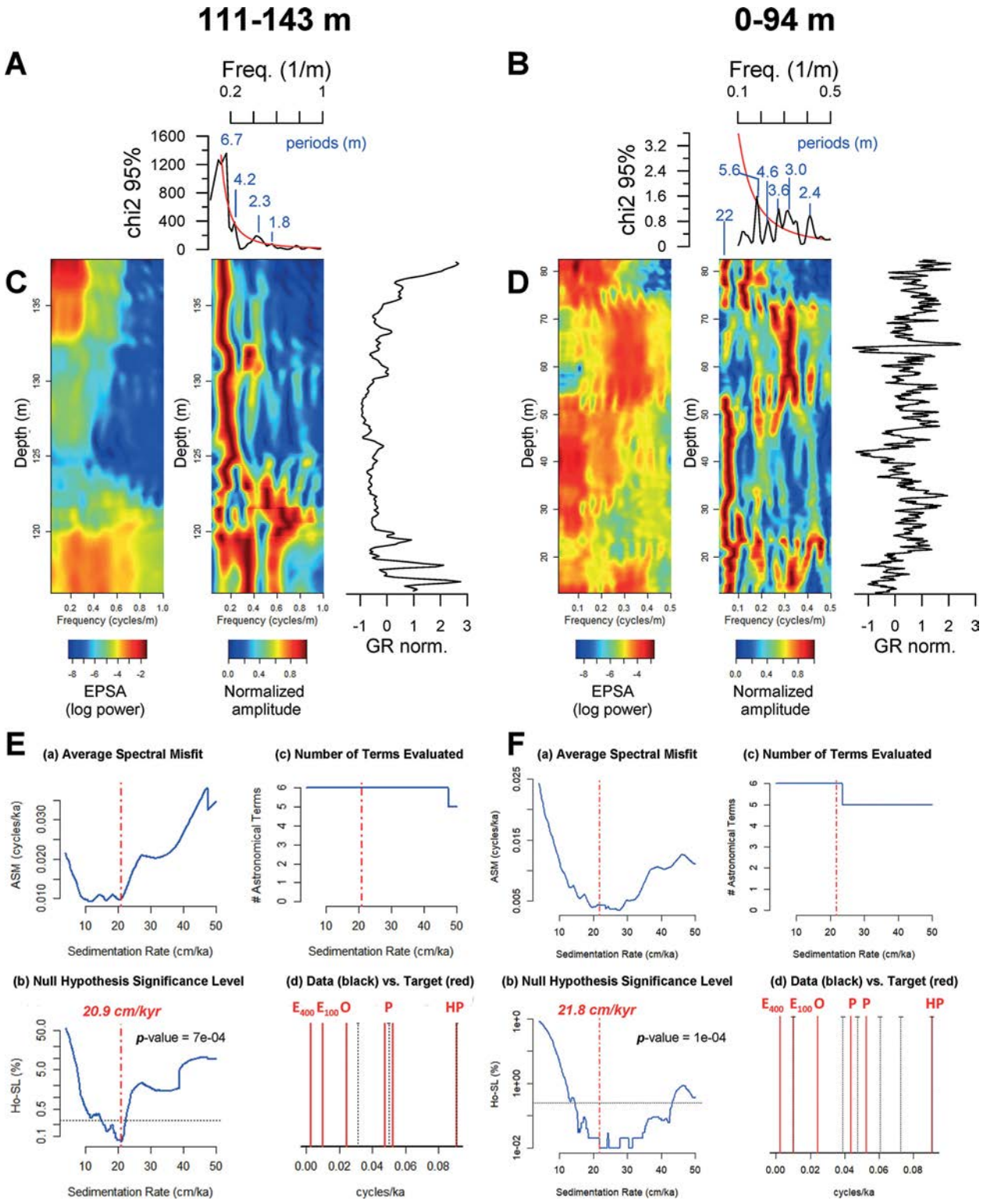
111-143 m
0-94 m
A
B
Freq. (1/m)
periods (m)
chi2 95%
6.7
4.2
2.3
1.8
5.6
4.6
3.0
3.6
2.4
22
C
D
Depth (m)
Frequency (cycles/m)
EPSA
(log power)
Normalized
amplitude
GR norm.
E
F
(a) Average Spectral Misfit
(c) Number of Terms Evaluated
ASM (cycles/ka)
Astronomical Terms
Sedimentation Rate (cm/ka)
(b) Null Hypothesis Significance Level
(d) Data (black) vs. Target (red)
20.9 cm/kyr
p-value = 7e-04
21.8 cm/kyr
p-value = 1e-04
Ho-SL (%)
E400 E100 O
P
HP
cycles/ka

Fig. 3. Time-series analysis results from the gamma-ray downhole log data from the FB2001 drillhole at Messel. Only the results from the Lower Messel Formation (LMF; depth section 143 m to 111 m depth) and Middle Messel Formation are shown (MMF; depth section 94 to 1 m depth; Fig. 1; cf. Sections 3 and 4 for more details); (**A** and **B**) REDFIT spectral analysis with the 95 % significance level marked by the red line; (**C** and **D**) Evolutive Harmonic Analysis (EHA). Dominant frequencies are marked by white dotted lines. Shown are the EHA amplitude (EPSA – evolutive power spectral analysis), EHA harmonic F-test with confidence levels set to the 95 % percentile, and the normalized gamma ray data. The maximum frequency is set to f_{max} = 1.0 and the window size was set to 25 m for the interval 1–94 m and 10 m for the section 143–111 m (cf. Section 3 for more details); (**E** and **F**) Results of Average Spectral Misfit (ASM) calculations for frequencies with >95 % confidence level in the gamma-ray spectrum using 10^4 iterations for 4–50 cm/kyr sedimentation rates (cf. Section 4.2 for more details). Relation of the spectral peaks (dashed black line; numbers indicate the respective periods in the depth domain) relative to the orbital target frequencies (red lines; E_{400} – long eccentricity, E_{100} – short eccentricity, O – obliquity, P – precession, HP – half-precession); black bars on top of spectral peaks denote the half-width of each peak. ASM calculation (black line) and the significance level estimation for null hypothesis rejection (SL-Ho, blue line) with critical significance level indicated (dotted line). The results indicate that the null-hypothesis of no orbital forcing can be rejected, with the average sedimentation rate noted accordingly (cf. Section 4.2 for further discussion).

~22 cm/kyr (Fig. 3), we find that all significant cycles of the oil-shale interval of the MMF relate either to the half-precession (~2.4 m, ~3.0 m and ~3.6 m) or precession (~4.6 m and ~5.6 m cycles) band-widths. It should be noted that due to the temporally restricted nature of the LMF and MMF oil-shale sections (c. 150 kyr and c. 420 kyr, respectively, based on their individual average sedimentation rates derived from the ASM; see Fig. 3), the relationship of the gamma-ray variability of these sections to short and long eccentricity cannot be assessed robustly using time-series analysis. Nevertheless, our results imply that the depositional changes within the LMF and MMF oil shales as documented by the gamma-ray record responded strongly to orbital (Milankovitch) cycles, and thus support the previously expressed notion that the deposition of the Messel oil shale was linked to past climate variability paced by orbital frequencies (Lenz et al. 2010, Lenz et al. 2011, Lenz et al. 2015). In addition, the similar average sedimentation rates for both oil-shale sections indicate that the depositional background conditions during both intervals were likely comparable, reflecting meromictic lake conditions (Felder and Harms 2004).

Interestingly, while half-precession and precession are clearly expressed in the ASM of the LMF and MMF oil-shale sections (Fig. 3), the obliquity imprint remains ambiguous as it is seemingly recorded in the LMF, but not the MMF. This is in line with previous pollen-based work on the FB2001 sediment core (Lenz et al. 2011). Our findings of a weak or missing obliquity imprint are in line with the general concept that the influence of obliquity on global climate during warm, ice-free periods such as the Eocene is weak, while the influence of eccentricity and precession is high (Zachos et al. 2001).

To produce an astronomical tuning, we filtered the precession signal from the gamma-ray data for both oil-shale intervals, respectively, using a taner filter (cf. Section 3.2 for more details). The precession filter for the oil-shale section of the LMF indicates c. 7 precession cycles with increasing amplitude from the base to the top of the section (Fig. 4). In contrast, the filter of the MMF oil shale consists of c. 28 cycles with a clearly expressed amplitude modulation, causing a bundling of 4–6 precession cycles (Fig. 4). We thus argue that the amplitude modulation represents short-eccentricity variability in the oil shale of the MMF, and assume that this might also be the case for the weakly expressed amplitude modulation in the LMF (Fig. 4). We then aligned the filtered precession signal and its implied short-eccentricity envelope to the eccentricity signal of the La2010d astronomical solution of Laskar et al. (2011). The La2010d solution was applied as it is considered to be particularly reliable back to 54 Ma (Hilgen et al. 2020, Lauretano et al. 2016, Westerhold et al. 2012). To identify the optimal tuning option, we further considered a set of prerequisite boundary conditions: We assume (i) that the LMF basis age is representative of the age of the maar-forming eruption, (ii) the eruption took place at 48.065 ± 0.21 Ma following the re-calibration of the $^{40}Ar/^{39}Ar$-age of the fish canyon tuff to 28.176 ± 0.023 Ma (Phillips et al. 2022), and (iii) that the LMF and MMF sediments present in the drillcore FB2001 cover together between ~0.65 Ma to ~1 Ma based on previous estimates (Felder and Harms 2004, Lenz et al. 2015). These assumptions assign the top of the MMF to an age between ~47.4 Ma and ~47.0 Ma.

Starting our tuning with the filtered precession signal of the MMF oil shale, we observe five inferred

short-eccentricity cycles that seemingly follow a long-term ~400 kyr eccentricity pattern. Given the aforementioned boundary conditions of the astronomical tuning, we argue that these five short-eccentricity cycles recorded in the MMF can only be reasonably placed between ~47.2 and ~47.6 Ma. Assuming an in-phase behaviour of the gamma-ray signal to orbitally paced climate variability, we aligned the mid-point gamma-ray short-eccentricity maxima directly to the mid-point short-eccentricity maxima of La2010d (Fig. 4; Tab. 1). In contrast, the temporal placement of the precession filter derived from the LMF oil shale is more difficult due to its shortness. A transition from the employed La2010d eccentricity tuning target to one of the other available eccentricity solutions, such as La2010a-c or Ze2020a-d (Laskar et al. 2011, Zeebe and Lourens 2022), would typically result in a maximum offset of <10 kyr for both the MMF and LMF (see Supplementary Figures 2–3). The sole exception to this is La2010a, which induces a shift of the LMF towards older ages by c. 50 kyr. However, considering the geological context of the LMF oil shale, nestled between both clastic layers, it implies an inherent tendency to exhibit more characteristics of a "floating time scale". Therefore, the potential offset of 50 kyr when tuning to La2010a as opposed to La2010d falls well within the expected uncertainty range for the chronological positioning of the LMF oil shale.

Generally, the progressive increase in precessional amplitude as captured in the LMF oil-shale filter seems

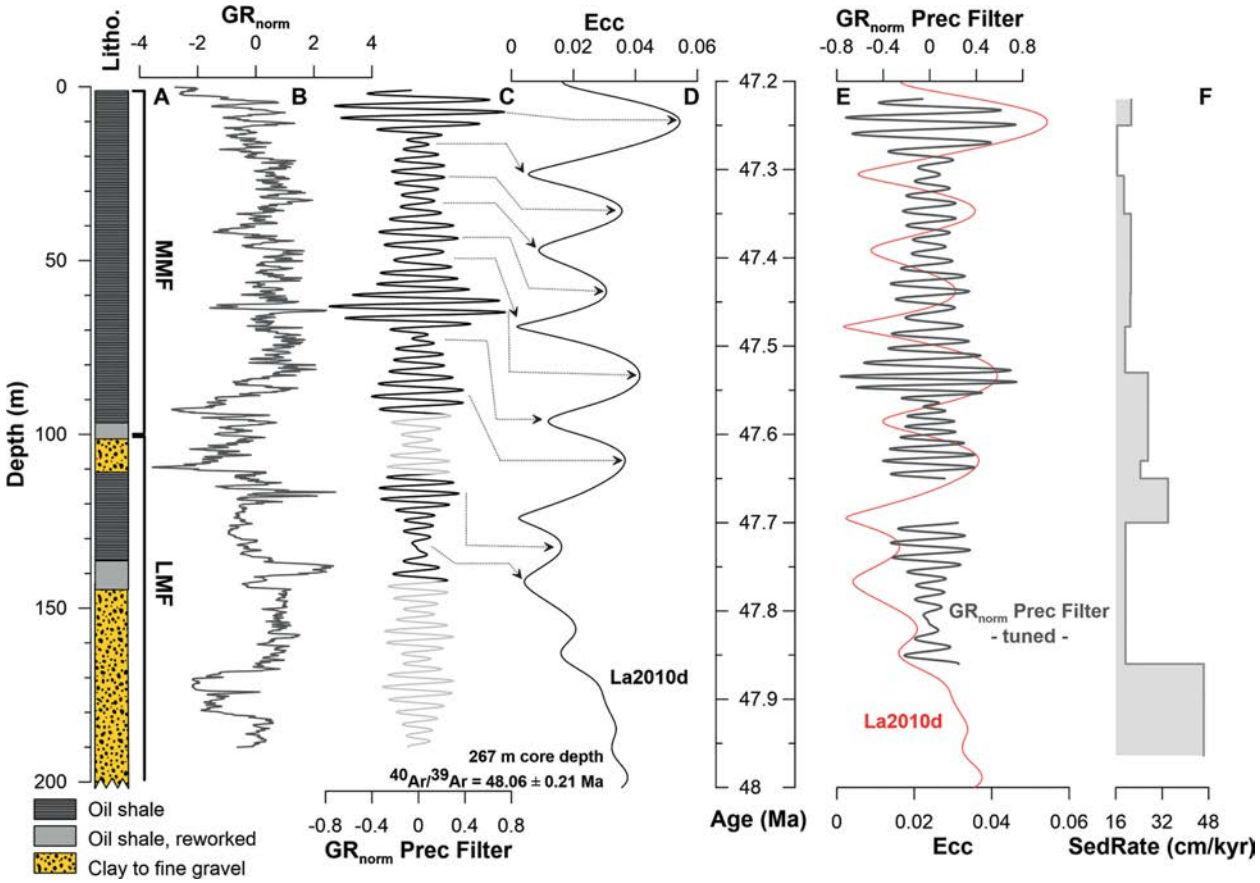

Fig. 4. Astronomical tuning of the Middle (MMF) and Lower Messel Formation (LMF) as recovered in the FB2001 drillcore (Felder and Harms 2004); (**A**) Generalized lithostratigraphy of the Messel FB2001 drillcore (modified after Felder and Harms 2004), (B) "normalized" gamma-ray downhole log data (GR) from the FB2001 drillhole (Felder and Harms 2004; cf. Section 3.2 for more details); (C) Precession (prec) filter derived from the "normalized" downhole gamma-ray signal at Messel (cf. Section 3.2 for details); (D) eccentricity (ecc) signal derived from astronomical solution La2010d (Laskar et al. 2011). Tuning tie points between the precession filter derived from the FB2001 "normalized" downhole gamma-ray in the depth domain and the La2010d solution are indicated by arrows (see Tab. 1; cf. Section 4.2 for more details); (**E**) Tuning fit of the eccentricity (ecc) astronomical solution La2010d (red line; Laskar et al. 2011) and the tuned precession filter derived from the FB2001 "normalized" borehole gamma-ray ´(black line; Felder and Harms 2004; cf. Section 3.2 for details); (**F**) Resulting sedimentation rate based on the proposed astronomical tuning.

to fit best to the increasing short-eccentricity amplitude between ~47.85 Ma to 47.7 Ma in the La2010d orbital solution (Fig. 4). This temporal placement would allocate c. 190 kyr of duration to the lower LMF clastic layer between 228 and 143 m underlying the LMF oil shale, and c. 150 kyr to the upper LMF clastic layer between 111 and 94 m overlying the LMF oil shale. In case of the lower LMF clastic layer, this would result in an average sedimentation rate of ~0.5 m/kyr for this section and thus represent a doubling of the sedimentation rate relative to the average sedimentation rates previously reported for the oil-shale sections (Lenz et al. 2015; Fig. 4). Based on this estimate, the lower LMF clastic layer spans c. 190 kyr. The palynological analysis of Lenz et al. (2007) revealed, however, the presence of pioneer vegetation (i. e., ferns) during this time interval. Based on Recent studies, the re-establishment of pioneer vegetation on volcanic substrates typically occurs rapidly within few decades or even less (e. g., Smathers and Mueller-Dombois 1974, and references therein). The calculated duration of c. 190 kyr is primarily influenced by the new calibration of the $^{40}Ar/^{39}Ar$ age at the base of the LMF, which has a larger error margin at 48.065 ± 0.21 Ma. It is thus important to highlight that, from a palynological perspective, the deposition of the oil-shale-free sediments between 228 m and 143 m core depth may have occurred at a considerably faster rate. This is consistent with the $^{40}Ar/^{39}Ar$ age when considering the associated error. The upper LMF clastic layer would also be characterized by increased sedimentation rates (~0.3 m/kyr), albeit not as pronounced as within the lower LMF clastic layer (Fig. 4). The higher sedimentation rates in both cases would align well with the previously argued debris-flow depositions associated with both intervals presumably caused by crater-flank instabilities (Felder and Harms 2004). In total, we thus argue that the LMF and MMF recovered in the FB2001 core contain c. 840 kyr between 48.06 Ma (corresponding to 228 m core depth) to 47.22 Ma (1 m core depth).

Based on our new astronomical tuning, we can also identify enhanced precession to half-precession interferences under high eccentricity in the lower part of the recovered MMF oil shale. This fact is also evident in the applied precession filter, which reveals two "additional" precession cycles within the two short-eccentricity cycles associated with the lower part of the MMF oil-shale relative to the middle and upper MMF oil-shale sections in the FB2001 core (Fig. 4). For Pleistocene boundary conditions, the half-precession signal has been linked to low-latitude climate variability such as monsoonal influence (Berger et al. 1997, Berger et al. 2006, Short et al. 1991, Ulfers et al. 2022). A strong low-latitude imprint would be in line with the previously proposed tropical monsoonal climate at mid-latitude Messel during the early to middle Eocene (Grein et al. 2011). Gleaning from the Pleistocene time period, eccentricity maxima would lead to a strengthened monsoon and increased precipitation associated with high (half)precession amplitudes, and *vice versa* for eccentricity minima (Ulfers et al. 2022, Zachos et al. 2010). In fact, this scenario would align with the observed increased sedimentation rates of the lower part of the MMF oil shale in FB2001 (~27 cm/kyr), which coincides with a ~400 kyr long-eccentricity maximum, while sedimentation rates of the middle section (~16 cm/kyr) in turn align with a ~400 kyr eccentricity minimum (Fig. 4). Strikingly, sedimentation rates do not increase again in the uppermost section of the MMF oil shale in FB2001, which is associated with the highest precession (and, by extension, eccentricity) amplitudes of the entire recovered MMF oil shale. This development is counterintuitive. However, it is in line with previous suggestions of a long-term trend towards less humid conditions across the MMF oil-shale interval in FB2001 (Lenz et al. 2011, Lenz et al. 2015). This might indicate that an additional climate-shaping mechanism at least partially overprinted the orbital climate forcing (cf. Section 4.4).

4.3. Comparison of the KBSB 2022 astronomical tuning with the previously published pollen tuning

Based on palynological changes identified in the FB2001 sediment core, Lenz et al. (2015) suggested two astronomical tuning solutions for the LMF and MMF recovered in the FB2001 drillhole. To compare our astronomical tuning to the existing age-model we adopted the age-depth tie points of Lenz et al. (2015), applied them to the gamma-ray data, and subsequently filtered the precessional signal based on our previous filter settings (Fig. 5). We find that application of the Lenz et al. (2015) tie points leads to the association of the highest precessional amplitudes with a ~400 long-eccentricity minimum and *vice versa*, which is at odds with the general concept that high/low precession amplitudes are intrinsically linked to high/low eccentricity (Fig. 5; Laskar et al. 2004, Laskar et al. 2011). Within the constraints of the tuning boundary condi-

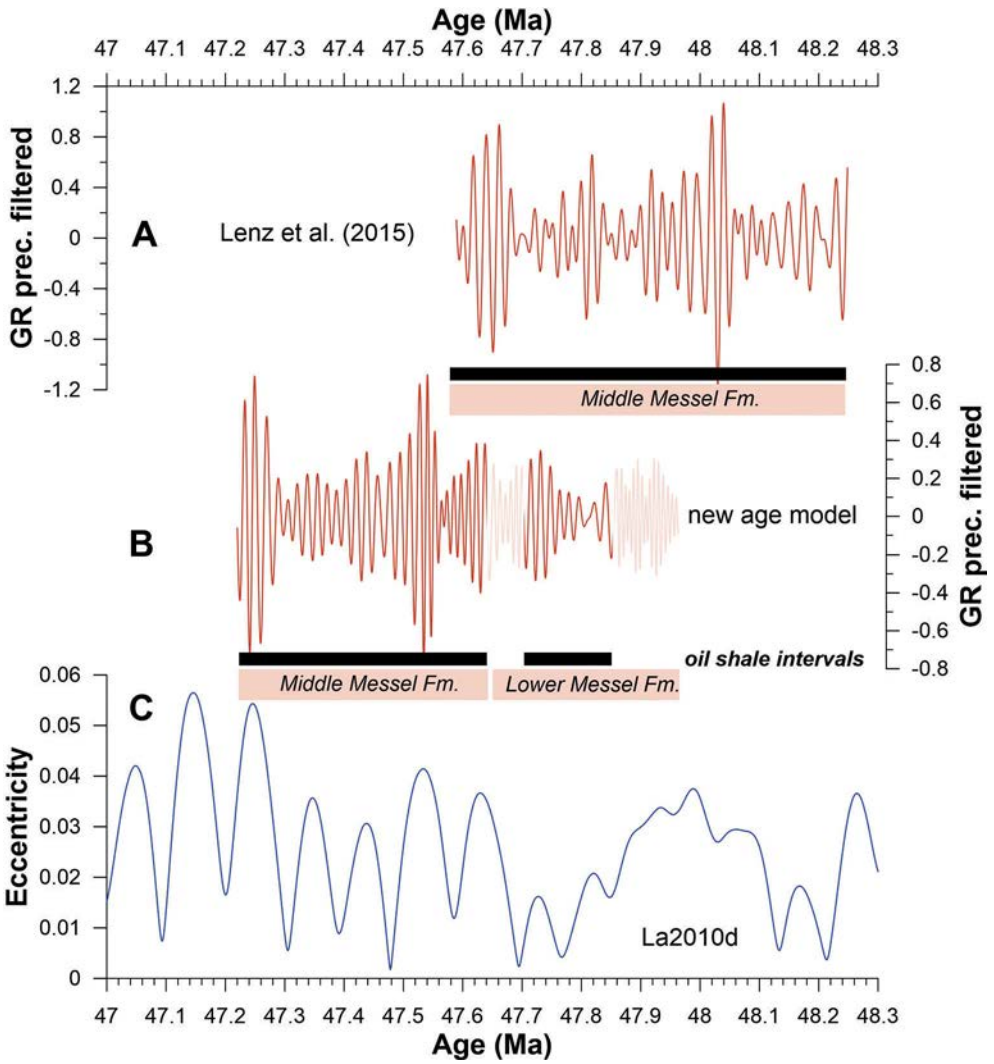

Fig. 5. Precession filter derived from the normalized downhole gamma-ray data from the Messel FB2001 drillcore (cf. Section 3.2 for details) using the age-depth tie points of (**A**) Lenz et al. (2015) and (**B**) this study. Filter settings utilized follow the description in Section 3; (**C**) Eccentricity variability (blue line) derived from the astronomical solution of La2010d (Laskar et al. 2011).

tions (cf. Section 4.2 for details), we thus argue that our tuning provides a better fit between the precessional amplitude modulation and the orbital La2010d solution than the Lenz et al. (2015) age model.

Additionally, distinct differences can be observed between both age models regarding the duration of the LMF and MMF. Firstly, the previously allocated total duration of the MMF oil shale in the FB2001 core of ~650 kyr is longer than the ~430 kyr as proposed in this study. Secondly, we estimate that the total duration of the LMF is c. 400 kyr, which in turn is longer than the previously proposed range of ~100 kyr to ~300 kyr (Lenz et al. 2015). The duration difference for both lithological units is most likely attributable to two aspects: (i) We argue that the lower LMF clastic layer underlying the LMF oil shale contains more time than previously considered because of the presence of c. 30 m of finely laminated clastic sediments from ~167 m upwards. This suggests that the progressive development of the Messel paleolake was closely recorded in the LMF clastic sedimentary sequence, and that at this point the earlier predominatant debris flow deposition had largely ceased. The decreasing abundance and thickness of the debrites is probably related to the increasing stability of the crater flanks (Felder and Harms 2004). (ii) We find only five clear short-eccentricity cycles (cf. Section 4.2 and Fig. 4) associated with the MMF oil shale in FB2001 instead

of five to six short-eccentricity cycles that have been suggested previously (Lenz et al. 2015). Particularly the latter might be a reflection of the different sensitivity of the underlying proxies to climate change. It is possible that the gamma-ray variability, which traces detrital input changes, responds more directly to climatic changes than the circum-lake vegetation that potentially records a buffered climatic signal due to (i) internal vegetational threshold and feedback mechanism (e. g., Webb 1986), and/or (ii) that a pollen depositional bias caused a dampening of the orbital signal incorporation into the sedimentary sequence (e. g., Li et al. 2018).

The average sedimentation rates of the LMF and MMF oil shales in FB2001 (~21 cm/kyr and ~22 cm/kyr, respectively) derived from our tuning also have implications for the proposed laminae thickness of the MMF. Previous suggestions were between ~14 cm/kyr (Schulz et al. 2002, Lenz et al. 2015) and ~15 cm/kyr (El Bay et al. 2002, Lenz et al. 2010) for the laminae sedimentation rates. Although our estimated sedimentation rates of ~20 cm/kyr are slightly higher, they are in line with earlier estimates of Goth et al. (1988) and Goth (1990), who also proposed sedimentation rates of up to 20 cm/kyr.

4.4. Messel – a potential archive of middle Eocene hyperthermals?

The aforementioned conundrum of overall reduced precipitation during deposition of the uppermost MMF oil shale in the FB2001 core, despite its temporal coincidence with a pronounced short-eccentricity maximum (cf. Section 4.2), was further investigated using previously published and new $\delta^{13}C_{TOC}$ data (Fig. 6). Within the Messel maar lake, $\delta^{13}C_{TOC}$ values have been argued to predominantly reflect changes in aquatic biomass (Bauersachs et al. 2014). In addition,

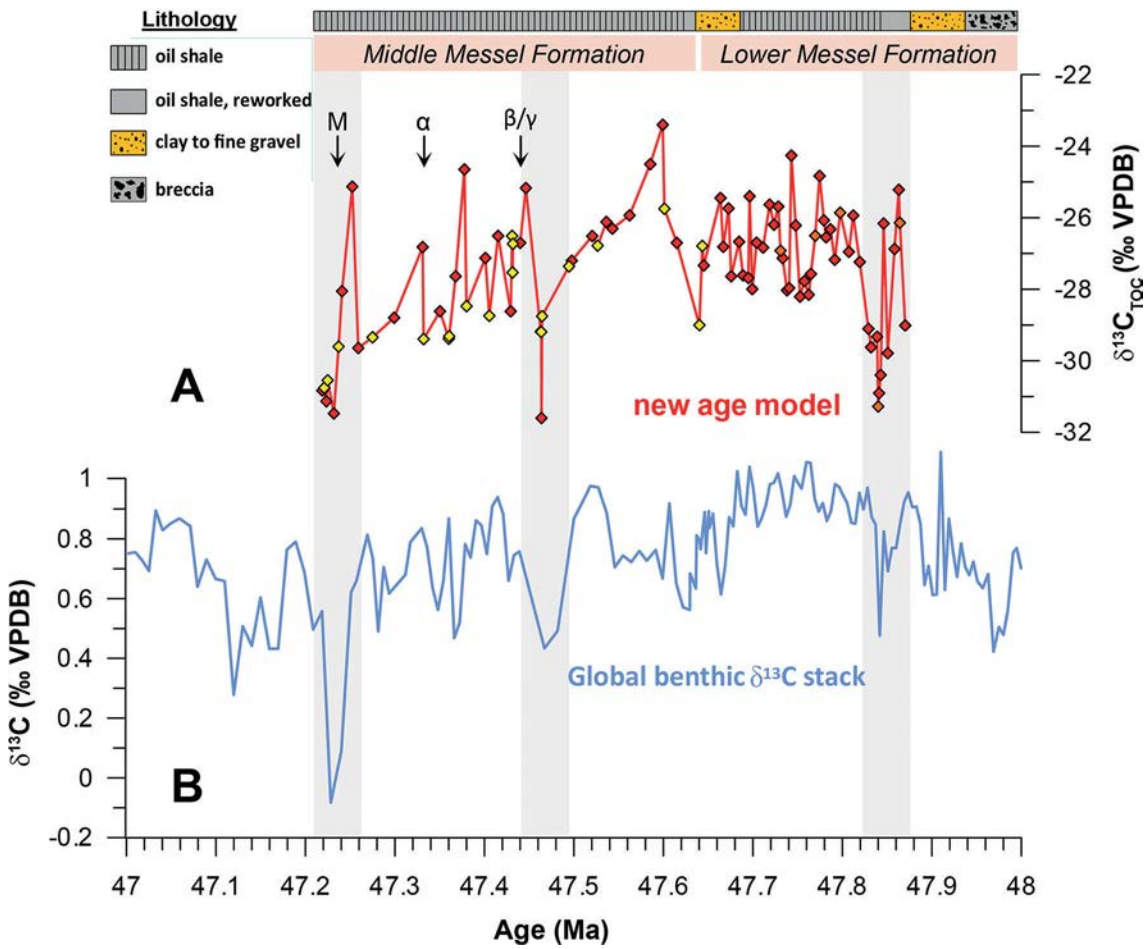

Fig. 6. Comparison of (**A**) the carbon-isotope values of the organic matter ($\delta^{13}C_{TOC}$) at Messel presented on the new astronomical tuning (red diamonds from Bauersachs et al. (2014), and yellow diamonds from this study; cf. Sections 3.5 and 4.4 for details) with (**B**) the global benthic $\delta^{13}C$ record (blue line) of Westerhold et al. (2020).

the presence of ^{13}C-depleted organic carbon may reflect the increased production of microbial (or volcanogenic) methane in the Messel maar lake, which would be reflected by characteristically low $\delta^{13}C$ values (Whiticar 1999) that are incorporated into the algal biomass via metabolizing the dissolved inorganic carbon sources of the lake water (Bauersachs et al. 2014).

The $\delta^{13}C_{TOC}$ trend along the FB2001 drillcore shifts from a median value of –26 ‰ at the onset of oil shale deposition in the LMF to –29 ‰ towards the top of the MMF (Fig. 6). Such negative $\delta^{13}C_{TOC}$ values are lower than the values for algae and photosynthetic bacteria in the Messel oil shale (~–22.5 ‰ and ~–24.5 ‰, respectively; Hayes et al. 1987), which might suggest more severe perturbations of the lake's carbon cycle possibly coupled to an increased injection and consumption of isotopically depleted carbon sources (such as deep-water derived methane and/or atmospheric CO_2 with a more ^{13}C-depleted signature than at present; Beaulieu et al. 2018, Harrison et al. 2017).

The long-term trend in ^{13}C depletion and the indication of a pronounced negative excursion in the $\delta^{13}C_{TOC}$ record are particularly interesting. These events occur more frequently in the upper section of the MMF oil-shale between 47.6 Ma and 47.2 Ma (Fig. 6), and their significance becomes apparent when considering the available global oceanic benthic $\delta^{13}C$ record (Fig. 6; Westerhold et al. 2020). Notably, we find a good fit between negative excursions in the global $\delta^{13}C$ CENOGRID stack and the $\delta^{13}C_{TOC}$ record from Messel (Fig. 6). It is important to note that this temporal match is not depended on the selection of our tuning target (compare Section 4.2.), and thus instead serves as an additional support for the validity of our age model. It also indicates that these global-scale events left an imprint on the isotopic composition of organic matter in the Messel paleolake. As negative $\delta^{13}C$ anomalies during the Paleogene are often associated with hyperthermals (Westerhold et al. 2020), we thus posit that $\delta^{13}C_{TOC}$ excursions in the LMF and MMF might represent the carbon-isotopic expression of hyperthermals. In this context, we also observe that the lithological marker beds in the LMF and MMF (M, α, β and γ; Fig. 6) are associated with negative $\delta^{13}C_{TOC}$ excursions (Fig. 6), which means that their deposition may not be related to temporally random processes such as volcanic eruptions as previously thought (Liesegang and Wuttke 2022), but instead are associated with orbitally driven climate change during the middle Eocene. However, further and more detailed research into the relationship between the carbon-isotope signals preserved in the Messel paleolake and global carbon-cycle dynamics is required to ground-truth the suggested link to global climate anomalies.

5. Conclusions

This study proposes a new astronomical tuning for the LMF and MMF lacustrine sedimentary sequences recovered in the FB2001 drillcore at the UNESCO World Heritage Site "Messel Fossil Pit" (Germany). Based on the new tuning, the recovered LMF and MMF sediments encompass a c. 840 kyr interval between 48.06 Ma and 47.22 Ma, with the oil shale of the MMF and LMF containing c. 430 kyr and c. 130 kyr, respectively. Intervals of coarse clastic sedimentation above and below the oil shale of the LMF comprise c. 150 kyr and c. 190 kyr, respectively. In comparison to the previously available age model of Lenz et al. (2015), our new age model results in a slightly shorter (by c. 200 kyr) duration of the recovered MMF section and a longer duration of the LMF section (by c. 100–200 kyr). As a consequence of the new tuning approach and a re-calibrated $^{40}Ar/^{39}Ar$ basal age of the LMF, the top of the recovered MMF has become slightly younger (by ~200 kyr; now 47.22 Ma) than suggsted previously. We estimate the average sedimentation rate for the laminae of the oil-shale intervals as ~20 cm/kyr, which is within the range of earlier estimates (Goth et al. 1988, Goth 1990).

Generally, our results confirm the perception that the sedimentary environment of the Messel paleolake was highly sensitive to variations in orbital forcing (Lenz et al. 2010, Lenz et al. 2011, Lenz et al. 2015). In detail, we find that the variability in the detrital contributions to the oil-shale as traced by the downhole gamma-ray log is governed by orbital precession and eccentricity. In this scenario, humid climate phases were characterized by lower TOC values and high gamma-ray values associated with high precession/eccentricity amplitudes, and *vice versa* for less humid climate conditions. However, in contrast to previous studies, we find no clear indication for the imprint of orbital obliquity on the gamma-ray data (Lenz et al. 2015).

Lastly, $\delta^{13}C_{TOC}$ anomalies in the record of the LMF and MMF sediments show a close match to the global deep-water $\delta^{13}C$ reference stack of Westerhold et al. (2020), arguing that perturbations in the global carbon cycle triggering hyperthermals may have left an im-

print on the organic matter deposited in the Messel paleolake. Overall, our data paint a picture of an orbital-scale variable climate during the early to middle Eocen.

Acknowledgements. David de Vleeschouwer and an anonymous reviewer are thanked for their constructive comments that helped to improve the manuscript. A. B. and S. K.-B. acknowledge DFG Grants BA 3809/16-1 and KA 4757/7-1, respectively. C. S., I. V., and A. M. acknowledge support through the VeWA consortium (Past warm periods as natural analogues of our 'highCO_2'-climate future) by the LOEWE programme of the Hessen Ministry of Higher Education, Research and the Arts, Germany. L. J. L. acknowledges the Netherlands Earth System Science Centre (NESSC), financially supported by the Ministry of Education, Culture, and Science (OCW) of the Netherlands. We thank S. Rheinberger for technical support during TOC analysis.

References

Acuna, E., Rico, P., & Acuna, M. E. (2009). Dprep: Data PreProcessing and Visualization Functions for Classification.

Anagnostou, E., John, E. H., Edgar, K. M., Foster, G. L., Ridgwell, A., Inglis, G. N., … Pearson, P. N. (2016). Changing atmospheric CO_2 concentration was the primary driver of early Cenozoic climate. *Nature*, *533* (7603), 380–384. https://doi.org/10.1038/nature17423

Bauersachs, T., Schouten, S., & Schwark, L. (2014). Characterization of the sedimentary organic matter preserved in Messel oil shale by bulk geochemistry and stable isotopes. *Palaeogeography, Palaeoclimatology, Palaeoecology*, *410*, 390–400. https://doi.org/10.1016/j.palaeo.2014.06.015

Berger, A., & Loutre, M. F. (1997). Intertropical latitudes and precessional and half-precessional cycles. *Science*, *278*(5342), 1476–1478. https://doi.org/10.1126/science.278.5342.1476

Berger, A., Loutre, M. F., & Mélice, J. L. (2006). Equatorial insolation: From precession harmonics to eccentricity frequencies. *Climate of the Past*, *2*(2), 131–136. https://doi.org/10.5194/cp-2-131-2006

Bijl, P. K., Bendle, J. A. P., Bohaty, S. M., Pross, J., Schouten, S., Tauxe, L., … Yamane, M. (2013). Eocene cooling linked to early flow across the Tasmanian Gateway. *Proceedings of the National Academy of Sciences of the United States of America*, *110*(24), 9645–9650. https://doi.org/10.1073/pnas.1220872110

Burke, K. D., Williams, J. W., Chandler, M. A., Haywood, A. M., Lunt, D. J., & Otto-Bliesner, B. L. (2018). Pliocene and Eocene provide best analogs for near-future climates. *Proceedings of the National Academy of Sciences of the United States of America*, *115*(52), 13288–13293. https://doi.org/10.1073/pnas.1809600115

Caballero, R., & Huber, M. (2013). State-dependent climate sensitivity in past warm climates and its implications for future climate projections. *Proceedings of the National Academy of Sciences of the United States of America*, *110* (35), 14162–14167. https://doi.org/10.1073/pnas.1303365110

Díaz-Curiel, J., Miguel, M. J., Biosca, B., & Arévalo-Lomas, L. (2021). Gamma ray log to estimate clay content in the layers of water boreholes. *Journal of Applied Geophysics*, *195*, 104481. https://doi.org/10.1016/j.jappgeo.2021.104481

El Bay, R., Jacoby, W., & Wallner, H. (2002). Milankovitch signals in Messel "Oilshales.". *Kaupia Darmstädter Beiträge zur Naturgeschichte*, *11*, 69–72.

Farquhar, G., Ehleringer, J. R., & Hubick, K. T. (1989). Carbon isotope discrimination and photosynthesis. *Annual Review of Plant Physiology and Plant Molecular Biology*, *40*(1), 503–537. https://doi.org/10.1146/annurev.pp.40.060189.002443

Felder, M., & Harms, F. J. (2004). Lithologie und genetische Interpretation der vulkano-sedimentären Ablagerungen aus der Grube Messel anhand der Forschungsbohrung Messel 2001 und weiterer Bohrungen. *Courier Forschungsinstitut Senckenberg*, *252*, 151–203.

Fertl, W. H., & Chilingar, G. V. (1988). Total organic carbon content determined from well logs. *SPE Formation Evaluation*, *3*(2), 407–419. https://doi.org/10.2118/15612-PA

Franzen, J. L., Weber, J., & Wuttke, M. (1982). Senckenberg-Grabungen in der Grube Messel bei Darmstadt. 3. Ergebnisse 1979-1981. *Courier Forschungsinstitut Senckenberg*, *54*, 1–118.

Goth, K. (1990). Der Messeler Ölschiefer ein Algenlaminit. *Courier Forschungsinstitut Senckenberg*, *131*, 1–143.

Goth, K., De Leeuw, J. W., Püttmann, W., & Tegelaar, E. W. (1988). Origin of Messel Oil Shale kerogen. *Nature*, *336* (6201), 759–761. https://doi.org/10.1038/336759a0

Grein, M., Utescher, T., Wilde, V., & Roth-Nebelsick, A. (2011). Reconstruction of the middle Eocene climate of Messel using palaeobotanical data. *Neues Jahrbuch für Geologie und Paläontologie Abhandlungen*, *260*, 305–318. https://doi.org/10.1127/0077-7749/2011/0139

Hammer, Ø., Harper, D. A., & Ryan, D. D. (2001). PAST: Paleontological statistics software package for education and data analysis. *Palaeontologia Electronica*, *4*, 1–9.

Harms, F. J., Aderhold, G., Hoffmann, I., Nix, T., & Rosenberg, F. (1999). Erläuterungen zur Grube Messel bei Darmstadt, Südhessen. *Schriftenreihe der Deutschen Geologischen Gesellschaft*, *8*, 181–222.

Hayes, J. M., Takigiku, R., Ocampo, R., Callot, H. J., & Albrecht, P. (1987). Isotopic compositions and probable origins of organic molecules in the Eocene Messel shale. *Nature*, *329*(6134), 48–51. https://doi.org/10.1038/329048a0

Hilgen, F., Zeeden, C., & Laskar, J. (2020). Paleoclimate records reveal elusive ~200-kyr eccentricity cycle for the first time. *Global and Planetary Change*, *194*, 103296. https://doi.org/10.1016/j.gloplacha.2020.103296

Hinsken, S., Ustaszewski, K., & Wetzel, A. (2007). Graben width controlling syn-rift sedimentation: The palaeogene southern upper rhine graben as an example. *International Journal of Earth Sciences*, *96*(6), 979–1002. https://doi.org/10.1007/s00531-006-0162-y

Hodell, D. A., Crowhurst, S. J., Lourens, L., Margari, V., Nicolson, J., Rolfe, J. E., … Wolff, E. W. (2023). A 1.5-million-year record of orbital and millennial climate variability in the North Atlantic. *Climate of the Past*, *19*(3), 607–636. https://doi.org/10.5194/cp-19-607-2023

Illies, J. H. (1972). The Rhine graben rift system-plate tectonics and transform faulting. *Geophysical Surveys*, *1*(1), 27–60. https://doi.org/10.1007/BF01449550

IPCC (2021). AR6 [The Physical Science Basis, Contribution of Working Group I to the Sixth Assessment Report of the Intergovernmental Panel on Climate Change.]. *Climatic Change*, 2021.

Irion, G. (1977). Der eozäne See von Messel. *Natur und Museum*, *107*, 213–218. https://doi.org/10.1007/978-3-642-57198-5_21

Kozdon, R., Kelly, D. C., Kita, N. T., Fournelle, J. H., & Valley, J. W. (2011). Planktonic foraminiferal oxygen isotope analysis by ion microprobe technique suggests warm tropical sea surface temperatures during the Early Paleogene. *Paleoceanography*, *26*(3), PA3206. https://doi.org/10.1029/2010PA002056

Laskar, J., Fienga, A., Gastineau, M., & Manche, H. (2011). La2010: A new orbital solution for the long-term motion of the Earth. *Astronomy & Astrophysics*, *532*, A89. https://doi.org/10.1051/0004-6361/201116836

Laskar, J., Robutel, P., Joutel, F., Gastineau, M., Correia, A. C. M., & Levrard, B. (2004). A long-term numerical solution for the insolation quantities of the Earth. *Astronomy & Astrophysics*, *428*(1), 261–285. https://doi.org/10.1051/0004-6361:20041335

Lauretano, V., Hilgen, F. J., Zachos, J. C., & Lourens, L. J., 2016. Astronomically tuned age model for the early Eocene carbon isotope events: A new high-resolution $\delta^{13}C_{benthic}$ record of ODP Site 1263 between ~49 and ~54 Ma. *Newsletters on Stratigraphy*, *49*, 383–400. https://doi.org/10.1127/nos/2016/0077

Lenz, O. K., & Wilde, V. (2018). Changes in Eocene plant diversity and composition of vegetation: The lacustrine archive of Messel (Germany). *Paleobiology*, *44*(4), 709–735. https://doi.org/10.1017/pab.2018.25

Lenz, O. K., Wilde, V., Mertz, D. F., & Riegel, W. (2015). New palynology-based astronomical and revised 40Ar/39Ar ages for the Eocene maar lake of Messel (Germany). *International Journal of Earth Sciences*, *104*(3), 873–889. https://doi.org/10.1007/s00531-014-1126-2

Lenz, O. K., Wilde, V., & Riegel, W. (2007). Recolonization of a Middle Eocene volcanic site: Quantitative palynology of the initial phase of the maar lake of Messel (Germany). *Review of Palaeobotany and Palynology*, *145*(3-4), 217–242. https://doi.org/10.1016/j.revpalbo.2006.11.001

Lenz, O. K., Wilde, V., & Riegel, W. (2011). Short-term fluctuations in vegetation and phytoplankton during the Middle Eocene greenhouse climate: A 640-kyr record from the Messel oil shale (Germany). *International Journal of Earth Sciences*, *100*(8), 1851–1874. https://doi.org/10.1007/s00531-010-0609-z

Lenz, O. K., Wilde, V., Riegel, W., & Harms, F. J. (2010). A 600 kyr record of El Niño-Southern Oscillation (ENSO): Evidence for persisting teleconnections during the Middle Eocene greenhouse climate of Central Europe. *Geology*, *38*(7), 627–630. https://doi.org/10.1130/G30889.1

Li, F., Gaillard, M. J., Xu, Q., Bunting, M. J., Li, Y., Li, J., … Shen, W. (2018). A review of relative pollen productivity estimates from temperate china for pollen-based quantitative reconstruction of past plant cover. *Frontiers in Plant Science*, *9*, 01214. https://doi.org/10.3389/fpls.2018.01214

Liesegang, M., & Wuttke, M. (2022). Lithogenesis of a phosphatized tephra marker horizon in the Eocene Messel maar lake. *International Journal of Earth Sciences*, *111*(7), 2225–2238. https://doi.org/10.1007/s00531-022-02241-x

Lorenz, V. (2003). Maar-diatreme volcanoes, their formation, and their setting in hard-rock or soft-rock environments. *Geolines (Praha)*, *15*, 72–83.

Lourens, L. J., Becker, J., Bintanja, R., Hilgen, F. J., Tuenter, E., van de Wal, R. S. W., & Ziegler, M. (2010). Linear and non-linear response of late Neogene glacial cycles to obliquity forcing and implications for the Milankovitch theory. *Quaternary Science Reviews*, *29*(1-2), 352–365. https://doi.org/10.1016/j.quascirev.2009.10.018

Mertz, D. F., & Renne, P. R. (2005). A numerical age for the Messel fossil deposit (UNESCO World Heritage Site) derived from $^{40}Ar/^{39}Ar$ dating on a basaltic rock fragment. *Courier Forschungsinstitut Senckenberg*, *255*, 67–75.

Meyers, S. R., (2014). astrochron: An R Package for Astrochronology.

Nazeer, A., Abbasi, S. A., & Solangi, S. H. (2016). Sedimentary facies interpretation of Gamma Ray (GR) log as basic well logs in Central and Lower Indus Basin of Pakistan. *Geodesy and Geodynamics*, *7*(6), 432–443. https://doi.org/10.1016/j.geog.2016.06.006

Pearson, P. N., van Dongen, B. E., Nicholas, C. J., Pancost, R. D., Schouten, S., Singano, J. M., & Wade, B. S. (2007). Stable warm tropical climate through the Eocene Epoch. *Geology*, *35*(3), 211–214. https://doi.org/10.1130/G23175A.1

Phillips, D., Matchan, E. L., Dalton, H., & Kuiper, K. F. (2022). Revised astronomically calibrated $^{40}Ar/^{39}Ar$ ages for the Fish Canyon Tuff sanidine – Closing the inter-laboratory gap. *Chemical Geology*, *597*, 120815. https://doi.org/10.1016/j.chemgeo.2022.120815

Poupon, A., & Gaymard, R. (1970). Evaluation of clay content from logs. Presented at the SPWLA ^{11}th Annual Logging Symposium. SPWLA-1970-G.

Pross, J., Contreras, L., Bijl, P. K., Greenwood, D. R., Bohaty, S. M., Schouten, S., … Brinkhuis, H. (2012). Persistent near-tropical warmth on the Antarctic continent during the early Eocene epoch. *Nature*, *488*(7409), 73–77. https://doi.org/10.1038/nature11300

R Core Team (2014). R: A language and environment for statistical computing.

Raddadi, M. C., Arnaud Vanneau, A., Poupeau, G., Carrio-Schaffhauser, E., Arnaud, H., & Rivera, A. (2005). Interpretation of gamma-ray logs: The distribution of uranium in carbonate platform. *Comptes Rendus Geoscience*, *337*(16), 1457–1461. https://doi.org/10.1016/j.crte.2005.08.009

Rae, J. W. B., Zhang, Y. G., Liu, X., Foster, G. L., Stoll, H. M., & Whiteford, R. D. M. (2021). Atmospheric CO_2 over the past 66 million years from marine archives. *Annual Review of Earth and Planetary Sciences*, *49*(1), 609–641. https://doi.org/10.1146/annurev-earth-082420-063026

Ring, S. J., Bocherens, H., Wings, O., & Rabi, M. (2020). Divergent mammalian body size in a stable Eocene greenhouse climate. *Scientific Reports*, *10*(1), 3987. https://doi.org/10.1038/s41598-020-60379-7

Schaal, S., Schmitz-Münker, M., & Wolf, H.-G. (1987). Neue Korrelationsmöglichkeiten von Grabungsstellen in der eozänen Fossillagerstätte Grube Messel. *Courier Forschungsinstitut Senckenberg*, *91*, 203–211.

Schulz, M., & Mudelsee, M. (2002). REDFIT: Estimatingred-noise spectra directly from unevenly spaced paleoclimatic time series. *Computers & Geosciences*, *28*(3), 421–426. https://doi.org/10.1016/S0098-3004(01)00044-9

Schulz, R., Harms, F. J., & Felder, M. (2002). Die Forschungsbohrung Messel 2001: Ein Beitrag zur Entschlüsselung der Genese einer Ölschieferlagerstätte. *Zeitschrift für Angewandte Geologie*, *48*, 9–17.

Schweizer, M. K., Steele, A., Toporski, J. K. W., & Fogel, M. L. (2007). Stable isotopic evidence for fossil food webs in Eocene Lake Messel. *Paleobiology*, *33*(4), 590–609. https://doi.org/10.1666/05079.1

Short, D. A., Mengel, J. G., Crowley, T. J., Hyde, W. T., & North, G. R. (1991). Filtering of milankovitch cycles by Earth's geography. *Quaternary Research*, *35*(2), 157–173. https://doi.org/10.1016/0033-5894(91)90064-C

Sluijs, A., Schouten, S., Donders, T. H., Schoon, P. L., Röhl, U., Reichart, G.-J., … Brinkhuis, H. (2009). Warm and wet conditions in the Arctic region during Eocene Thermal Maximum 2. *Nature Geoscience*, *2*(11), 777–780. https://doi.org/10.1038/ngeo668

Smathers, G. A., & Mueller-Dombois, D. (1974). Invasion and recovery of vegetation after a volcanic eruption in Hawaii. *Natl. Park Serv. Sci. Monogr. Ser.*, *5*, 129.

Smith, K. T., Schaal, S., & Habersetzer, J. (Eds.). (2018). *Messel – An Ancient Greenhouse Ecosystem* (p. 355). Senckenberg Bücher.

Ulfers, A., Zeeden, C., Voigt, S., Sardar Abadi, M., & Wonik, T. (2022). Half-precession signals in Lake Ohrid (Balkan) and their spatio-temporal relations to climate records from the European realm. *Quaternary Science Reviews*, *280*, 107413. https://doi.org/10.1016/j.quascirev.2022.107413

Webb, T., III. (1986). Is vegetation in equilibrium with climate? How to interpret late-Quaternary pollen data. *Vegetatio*, *67*(2), 75–91. https://doi.org/10.1007/BF00037359

Weber, J. W. (1988). Sedimentpetrographische Untersuchungen in der eozänen Messel-Formation. Frankfurt (Main) Universität, Dissertation.

Wedmann, S., Bradler, S., & Rust, J. (2007). The first fossil leaf insect: 47 Million years of specialized cryptic morphology and behavior. *Proceedings of the National Academy of Sciences of the United States of America*, *104*(2), 565–569. https://doi.org/10.1073/pnas.0606937104

Wedmann, S., Hörnschemeyer, T., Engel, M. S., Zetter, R., & Grímsson, F. (2021). The last meal of an Eocene pollen-feeding fly. *Current Biology*, *31*(9), 2020–2026. https://doi.org/10.1016/j.cub.2021.02.025

Westerhold, T., Marwan, N., Drury, A. J., Liebrand, D., Agnini, C., Anagnostou, E., … Zachos, J. C. (2020). An astronomically dated record of Earth's climate and its predictability over the last 66 million years. *Science*, *369*(6509), 1383–1387. https://doi.org/10.1126/science.aba6853

Westerhold, T., Röhl, U., & Laskar, J. (2012). Time scale controversy: Accurate orbital calibration of the early Paleogene. *Geochemistry, Geophysics, Geosystems*, *13*(6), Q06015. https://doi.org/10.1029/2012GC004096

Whiticar, M. J. (1999). Carbon and hydrogen isotope systematics of bacterial formation and oxidation of methane. *Chemical Geology*, *161*(1-3), 291–314. https://doi.org/10.1016/S0009-2541(99)00092-3

Wonik, T. (2005). Erste Ergebnisse der geophysikalischen Messungen in der Forschungsbohrung Messel 2001. *Courier Forschungsinstitut Senckenberg*, *255*, 11–20.

Zachos, J., Pagani, M., Sloan, L., Thomas, E., & Billups, K. (2001). Trends, rhythms, and aberrations in global climate 65 Ma to present. *Science*, *292*(5517), 686–693. https://doi.org/10.1126/science.1059412

Zachos, J. C., McCarren, H., Murphy, B., Röhl, U., & Westerhold, T. (2010). Tempo and scale of late Paleocene and early Eocene carbon isotope cycles: Implications for the origin of hyperthermals. *Earth and Planetary Science Letters*, *299*(1-2), 242–249. https://doi.org/10.1016/j.epsl.2010.09.004

Zeebe, R. E., & Lourens, L. J. (2022). Geologically constrained astronomical solutions for the Cenozoic era. *Earth and Planetary Science Letters*, *592*, 117595. https://doi.org/10.1016/j.epsl.2022.117595

Zeileis, A., & Grothendieck, G. (2005). Zoo: S3 infrastructure for regular and irregular time series. *Journal of Statistical Software*, *14*(6), 1–27. https://doi.org/10.18637/jss.v014.i06

Zhu, J., Poulsen, C. J., & Tierney, J. E., (2019). Simulation of Eocene extreme warmth and high climate sensitivity through cloud feedbacks. *Sciience Advamces*, *5*, eaax1874. https://doi.org/10.1126/sciadv.aax1874

Manuscript received: July 17, 2023
Revisions required: October 13, 2023
Revised version received: November 03, 2023
Manuscript accepted: November 06, 2023

The pdf version of this paper includes an electronic supplement

Please save the electronic supplement contained in this pdf-file by clicking the blue frame above. After saving rename the file extension to .zip (for security reasons Adobe does not allow to embed .exe, .zip, .rar etc. files).

Table of contents – Electronic Supplementary Material (ESM)